Turk J Phys
35 (2011) , 13 – 22.

doi:10.3906/fiz-0907-21

Effect of nitrogen incorporation on the electronic and optical properties of AlGaAsN/GaAs quantum well lasers

Boualem MERABET, Abdelhadi LACHEBI and Hamza ABID
Applied Materials Laboratory, Researchs Center, Sidi Bel Abbes University, 22000, ALGERIA
e-mail: boualem19985@yahoo.fr

Received 20.11.2010

Abstract

In order to investigate the profound effect of small amounts of nitrogen incorporated into the III-V systems on the fundamental band gap, which decreases dramatically with increasing of N^+ implantation, we present a pseudopotential formalism within the Virtual Crystal Approximation confronted to the Band Anti-crossing model, which parameterizes successfully such behaviour, so as to study the electronic and optical properties of dilute $Al_xGa_{1-x}As_{1-y}N_y$ materials, prepared by implantation of N^+ into epitaxial AlGaAs. Analytical formulas of quantized energy levels in AlGaAsN quantum well (QW) lasers and optical transition wavelengths between subbands are presented and compared to simulations based on our programs.

Key Words: III-N-V; AlGaAsN, EPM, BAC, QW lasers, energy levels

1. Introduction

Over the last few years, group III nitrides and their alloys have attracted a great deal of attention as being among the most important materials systems for optoelectronic and electronic applications [1]. The band gap of the III-N-V systems depending strongly on the N-content as well as their lattice parameter and their electron effective mass has made of these alloys attractive materials for long wavelength vertical cavity surface emitting lasers (LW-VCSELs) and high efficiency hybrid solar cell applications [2–4]. The InP-based systems have been the source for wide reach applications, but due to low electron confinement they have poor high-temperature characteristics and their cost remains too high to design a high volume modern data communication networks. As such, the GaAs-based systems were proposed as an alternative to the InP-based ones to solve the above problems and a novel material for optoelectronics has been adopted, AlGaAsN [5, 6], which has not been studied as extensively as other narrower band gap III-N-V systems such as its homologous InGaAsN [7, 8]. The GaAs-based dilute group III-AsN materials systems with nitrogen content in the few percent range have attracted considerable current interest because of their use as active material in optoelectronic devices such as VCSELs on GaAs emitting at 1.3 μm [9].

Shan et al. [10] and Perkins et al. [11] have investigated the strong dependence of the fundamental gap on N-content in the III-N-V systems and attributed the additional feature (a new absorption edge above the fundamental band gap) observed in the optical spectrum of InGaAsN alloys to an anticrossing interaction between the localized N states and the extended states of the host semiconductor matrix [3], splitting the conduction band (CB) into two (upper and lower) subbands. This so-called band-anti crossing (BAC) model suggest that the reduction of the fundamental gap is due to the downward shift of the lower subband and the dispersion relations for both upper and lower conduction subbands are expressed as [12, 13]

$$E_{\pm}(k) = \frac{1}{2}\left\{[E_M(k) + E_N] \pm \sqrt{[E_M(k) - E_N]^2 + 4C_{MN}^2 y}\right\}, \tag{1}$$

where E_N is the N-energy level, $E_M(k)$ is the dispersion relation for the host SC matrix, y is the N-content and C_{MN} is the matrix element describing the coupling between N states and the extended states. Here, the gap E_- of $Al_xGa_{1-x}As_{1-y}N_y$ alloys can be given by [14]

$$E_- = \frac{1}{2}\left[(E_{gAl_xGa_{1-x}As} + E_N) - \sqrt{\left[E_{gAl_xGa_{1-x}As} - E_N\right]^2 + 4C_{MN}^2 y}\right]. \tag{2}$$

C_{MN} depending on the electronegativity difference between N and the group V of the host matrix does not depend on the Al fraction in AlGaAsN and equals to 2.7eV [3].

The empirical pseudopotential method (EPM) has gained recognition as being among the most important theoretical studies which have attributed the observed changes in the CB structure in the group III-N-V alloys to N-induced interactions between the extended states of Γ, L and /or X minima [15]. EPM has proved to be a powerful tool for understanding the electronic energy band structures (EBS) of the SCs. This method is mainly used to avoid some of first principles calculations difficulties (such the computationally time consuming) and to produce results that are in good agreement with experimental values [16, 17].

The aim of this work is to clarify the electronic and optical properties of $Al_xGa_{1-x}As_{1-y}N_y$ alloys and calculate the optical transition wavelength between the quantized energy levels in $Al_xGa_{1-x}As_{1-y}N_y$/GaAs QW lasers. Reaminder of this paper is organized as follows. In section 2, we have applied an EPM calculation to $Al_xGa_{1-x}As_{1-y}N_y$ alloys within the virtual crystal approximation (VCA), which we are confronted to the BAC model prediction. In Section 3, analytical expressions for the quantized energy levels in the $Al_xGa_{1-x}As_{1-y}N_y$ QW lasers are derived and numerical calculations are presented. Finally, our work is summarized in Section 4.

2. Calculations

The empirical pseudopotential parameters of a SC are defined as a superposition of both local and nonlocal of pseudo atomic potential of the form $V = V_L + V_{NL}$, where the non-local part (V_{NL}) has been omitted in this calculation. The pseudo-potential Hamiltonian $H = (-h/2m)\nabla^2 + V_L(\boldsymbol{r})$ contains an effective potential which is expanded as Fourier series in reciprocal lattice space [16–18]. The lattice constant of AlGaAsN obey this law:

$$a_{AlxGa1-xAs1-yNy} = (1-x)(1-y)a_{GaAs} + (1-x)ya_{GaN} + x(1-y)a_{AlAs} + xya_{AlN}, \tag{3}$$

where a_{GaAs}, a_{GaN}, a_{AlAs} and a_{AlN} are the lattice constants of the binary systems of AlGaAsN.

According to the VCA approximation [18], the pseudopotential form factors (PPFFs) for our alloys can be given by a sum of non linear combinations:

$$V^{s,a}_{Al_xGa_{1-x}As_{1-y}N_y} = (1-x)(1-y)V^{s,a}_{GaAs} + (1-x)yV^{s,a}_{GaN} + x(1-y)V^{s,a}_{AlAs}a_{AlAs} + xyV^{s,a}_{AlN}. \quad (4)$$

The alloy potential is calculated within the VCA approximation. To the VCA potential $V_{VCA}(\mathbf{r})$ we add a non-periodic potential $V_{dis}(\boldsymbol{r})$ due to the compositional disorder as

$$V^{(r)}_{alloy} = V^{(r)}_{VCA} + V^{(r)}_{dis}. \quad (5)$$

According to Lee et al. [19], the potential of $\mathrm{Al}_x\mathrm{Ga}_{1-x}\mathrm{As}_{1-y}\mathrm{N}_y$ is determined by taking into account of two kinds of disorder effect, the AlGa and the AsN disorders (C_{Al-Ga} and C_{As-N}) due to the random distribution of the Al and Ga atoms in the cationic sublattice and the As and N atoms in the anionic sublattice, respectively. $V_{alloy}(\boldsymbol{r})$ is given by

$$V_{alloy}(r) = V_{VCA}(r) + V_{1dis}(r) + V_{2dis}(r) = V_{VCA}(r) + x(1-x)C_{Al-Ga} + y(1-y)C_{As-N} \quad (6)$$

After developing this later relationship, we obtain $V_{VCA}(\boldsymbol{r})$ as:

$$\begin{aligned} V_{VCA}(r) &= [xy^2\frac{\Omega_{AlN}}{\Omega_{alloy}} + xy(1-y)\frac{\Omega_{AlAs}}{\Omega_{alloy}}]V_{AlN}(r) + [(1-x)y^2\frac{\Omega_{GaN}}{\Omega_{alloy}} + \frac{\Omega_{GaAs}}{\Omega_{alloy}}(1-x)(1-y)y]V_{GaN}(r) \\ &+[xy(1-y)\frac{\Omega_{AlN}}{\Omega_{alloy}} + x(1-y)^2\frac{\Omega_{AlAs}}{\Omega_{alloy}}]V_{AlAs}(r) + [(1-x)(1-y)y\frac{\Omega_{GaN}}{\Omega_{alloy}} + \\ &(1-x)(1-y)^2\frac{\Omega_{GaAs}}{\Omega_{alloy}}]V_{GaAs}(r) \end{aligned} \quad (7)$$

where Ω_{alloy}, Ω_{AlN}, Ω_{AlAs}, Ω_{GaN}, and Ω_{GaAs} are, respectively, the volumes of the alloy and the binary systems AlN, AlAs, GaN and GaAs.

The non-periodic potentials V_{1dis} and V_{2dis} can be expressed as

$$\begin{aligned} V_{1dis}(r) &= -p_1[x(1-x)]^{0.5}\frac{1}{\Omega_{alloy}}\{[y^2\Omega_{AlN} + y(1-y)\Omega_{AlAs}]V_{AlN}(r) \\ &+[y(1-y)\Omega_{AlN} + (1-y)^2\Omega_{AlAs}]V_{AlAs}(r) - [y^2\Omega_{GaN} + y(1-y)\Omega_{GaAs}]V_{GaN}(r) \\ &-[y(1-y)\Omega_{GaN} + (1-y)^2\Omega_{GaAs}]V_{GaAs}(r)\} \end{aligned} \quad (8)$$

and

$$\begin{aligned} V_{2dis}(r) &= -p_2[y(1-y)]^{0.5}\frac{1}{\Omega_{alloy}}\{[x^2\Omega_{AlN} + x(1-x)\Omega_{GaN}]V_{AlN}(r) \\ &+[x(1-x)\Omega_{AlN} + (1-x)^2\Omega_{GaN}]V_{GaN}(r) - [x^2\Omega_{AlAs} + x(1-x)\Omega_{GaAs}]V_{AlAs}(r) \\ &-[x(1-x)\Omega_{AlAs} + (1-x)^2\Omega_{GaAs}]V_{GaAs}(r)\}, \end{aligned} \quad (9)$$

with p_1 and p_2 adjustable parameters which are varied until agreement was achieved with the BAC model predictions. Our quaternaries have been studied mainly for N-content $0.01 \leq y \leq 0.04$, a range where we expect to get good optic qualities of the AlGaAsN thin films used in QW lasers. The lattice-matched $\mathrm{Al}_x\mathrm{Ga}_{1-x}\mathrm{As}_{1-y}\mathrm{N}_y$

alloys on GaAs substrate is achieved by the relationship: $y = 0.0073\ x / (1.158 + 0.1274\ x)$, with $0 \leq y \leq 0.6\%$ and $0 \leq x \leq 1$. However, when this lattice-matching condition is not satisfied ($y > 0.6$ %), the lattice mismatch of AlGaAsN to GaAs is $\frac{\Delta a}{a_{GaAs}} = \frac{a_{Alloy} - a_{GaAs}}{a_{GaAs}} 100\%$, with a_{alloy} and a_{GaAs} the lattice constants of the $Al_x Ga_{1-x} As_{1-y} N_y$ alloy and GaAs, respectively. In Table 1, we have listed our adjusted local PPFFs (in Ryd) together with the lattice constants of Al(N, As) and Ga(N, As) binaries. The calculated band gap of each binary compound compared with the available experiment and/or other calculations are listed in Table 2. Assuming the VB top as energy zero, we have plotted the calculated EBS of the zinc-blende $Al_x Ga_{1-x} As_{1-y} N_y$ alloy (Figure 1) for $x = 0.05$ and $y = 0.01$, as a representative example, compared to the GaAs ones (Figure 2). The much more complicated behaviour of CB states is due to the fact that the CBs are more delocalized than the VBs, and the minima of the lowest CB shifted downward at the Γ point leads to a reduction of the fundamental band gap. This is believed due to the large electronegativity of N incorporated in small amounts in AlGaAs which shifts practically all the bands, such behaviour can then be parameterized successfully by the BAC model [20]. In comparison between the EBSs of GaAs and $Al_{0.05} Ga_{0.95} As_{0.99} N_{0.01}$, one can point out that no N-induced change in location of the VBs nature is noticed, while the CBs are extremely delocalized for only 1% of N-content (y). As can be seen from Figure 3 illustrating the computed gaps of $Al_x Ga_{1-x} As_{1-y} N_y$ for y up to 0.04, the indirect band gap E_g^X is the lowest, and then our alloys remain indirect gap. Hence, E_0 the fundamental energy gap of $Al_x Ga_{1-x} As_{1-y} N_y$ becomes narrower by more N^+ incorporation, which might lead to interesting applications of these alloys in infrared activity. From the fit of the energy band gaps data by a least-squares procedure, the expressions of the computed gaps (in eV) are:

$$E^{\Gamma} = 1.38 - 10.1y - 24.76y^2 \tag{10}$$

$$E^{L} = 1.28 - 1.27y - 8.38y^2 \tag{11}$$

$$E^{X} = 0.56 - 2.1y - 3.09y^2. \tag{12}$$

Accordingly, one can point out that a crossover between the direct and the X-indirect band gap in found to occur at $y = 0.084$, which corresponds to the band gap energy of 0.362 eV. If we happen to produce $Al_x Ga_{1-x} As_{1-y} N_y$ materials with good optical qualities with such a mole fraction of N without damaging the thin films as active layers, QWs with a direct band gap will be obtained. Figure 4 shows the fundamental band gap between the VB maxima and the CB minima (E _) as a function of N-fraction in $Al_{0.05} Ga_{0.95} As_{1-y} N_y$ within the BAC model compared to the E_0 band gap energy at Γ, the symmetry point, from the EPM method within the VCA approximation for y up to 4%. When the disorder potential is taken account for $p_1 = 0.395$ and $p_2 = 0.125$, excellent agreement with BAC data has been obtained for $y \leq 0.02$. From the quadratic terms (equations 10 to 12) one can note that the optical band gap bowing behaviour occurs differently for the Γ, X, and L-energy gaps and all these energy gaps show a downward bowing, but a giant Γ-bowing of –25 was found. This is mainly attributed to the localisation of the valence charge around N atoms, which is due to the large difference in electronegativity between N and As atoms. For the same bowing in both BAC and EPM calculations (p_1 ; p_2) are adjusted to be (0.375; –0.3).

Table 1. The adjusted local PPFFs (in q^{Ry}) and lattice constants (in nd) used in the calculation.

PPFFs	GaAs	GaN	AlAs	AlN
Vs(3)	-0.239833	-0.346925	-0.253800	-0.309603
Vs(8)	0.060536	0.161439	0.007100	0.280000
Vs(11)	0.012600	-0.016000	0.006200	0.112783
Va(3)	0.050000	0.200000	0.059000	0.330000
Va(4)	0.059625	0.211824	0.100500	0.067538
Va(11)	0.010000	0.135000	0.004500	0.015000
a (Å)	5.6531 [a]	4.5000 [b]	5.6542 [c]	4.3752 [d]

Note: [a,c,d] ref. [16]; [b] refs. [17, 28].

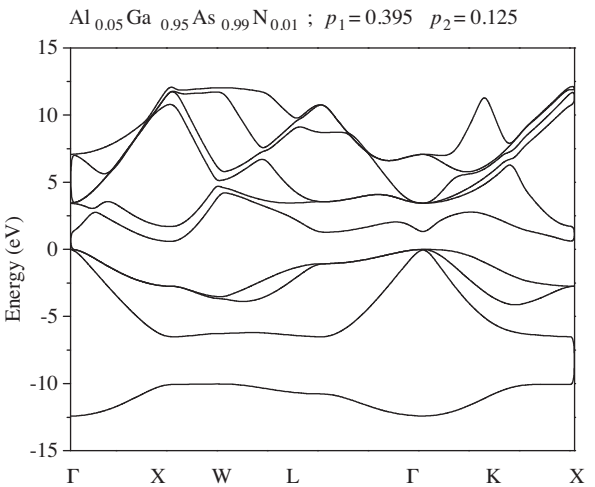

Figure 1. Energy band-structure of the $Al_xGa_{1-x}As_{1-y}N_y$ quaternary alloy for $x = 0.05$ and $y = 0.01$.

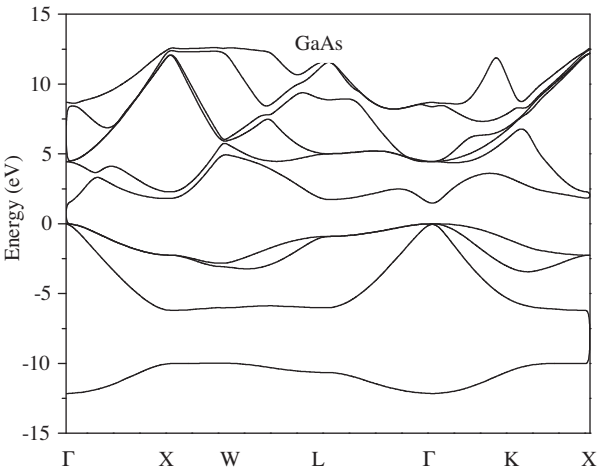

Figure 2. Energy band-structure of the GaAs binary compound.

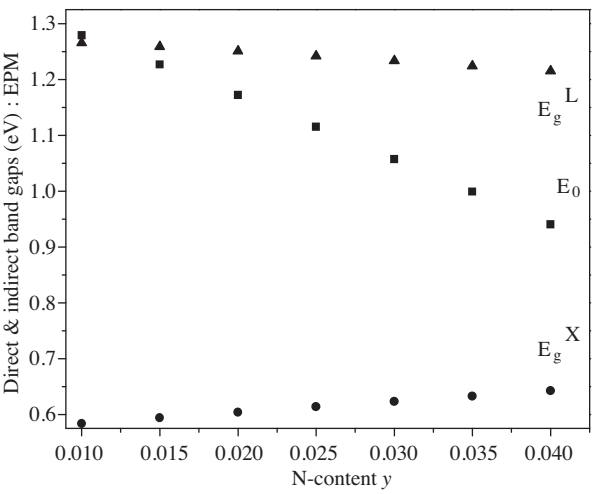

Figure 3. Γ, X, and L (direct and indirect) gap energies for $Al_{0.05}Ga_{0.95}As_{1-y}N_y$ alloys with $0.01 \leq y \leq 0.04$.

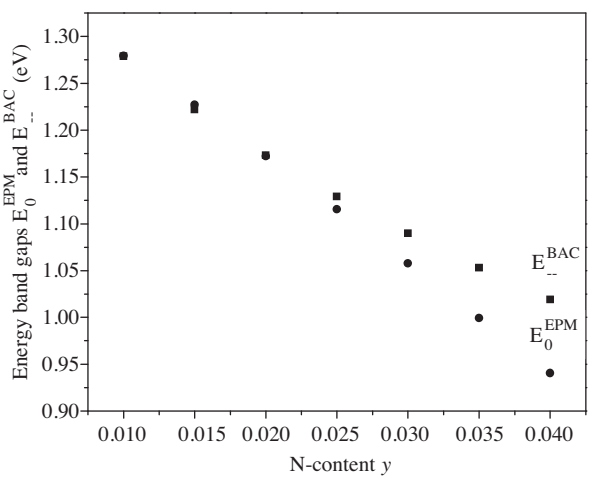

Figure 4. Band gap energies (E_0) calculated by EPM compared to those of the BAC model (E_{--}) for $Al_{0.05}Ga_{0.95}As_{1-y}N_y$ alloys with $0.01 \leq y \leq 0.04$.

Table 2. Comparison of the calculated direct and indirect gap energies (in eV) with experiment and other works.

Band gap		GaAs	GaN	AlAs	AlN
$\mathbf{E}_0$	Our cal.	1.421	3.306	2,951	6.006
	Others	1.523 [a]	3.24 [b]	3.057 [a]	5.4 [c]
	Exp.	1.42 [d]	3.2 [e]	3.13 [f]	6.2 [g]
$\mathbf{E}_g^X$	Our cal.	1.814	4.603	2.148	4.908
	Others	1.999 [a]	4.7 [a,b]	2.146 [a]	4.918 [a]
	Exp.	1.81 [d]		2.153[f]	
$\mathbf{E}_g^L$	Our cal.	1.723	6.046	2.794	9.304
	Others	1.814 [a]	6.04 [b]	2.525 [a]	9.079 [a]
	Exp.	1.72 [d]			

Note: [a] ref. [16]; [b] ref. [17]; [c] ref. [28]; [c] ref. [28]; [d] ref. [29]; [e] ref. [30]; [f] ref. [31]; [g] ref. [32].

As for the refractive index n designing QW lasers as well as solar cell applications, it can be determined using the Harrison model [21], where the optical high frequency (ε_∞) dielectric constant, according to the relationship $\varepsilon_\infty = n^2$, is related to the static dielectric constant ε_o by

$$\frac{\varepsilon_0 - 1}{\varepsilon_\infty - 1} = 1 + \alpha_p^2 \{1 + \frac{\alpha_p^2 \left[1 + 2\left(1 - \alpha_p^2\right)\right]}{2\left(1 - \alpha_p^2\right)^2}. \tag{13}$$

where α_p is the polarity defined by Vogl [22] as $\alpha_p = -V^a(3)/V^s(3)$, $V^s(3)$ and $V^a(3)$ are the symmetric and anti symmetric PPFFs at the reciprocal lattice vector $\mathbf{G}(111)$ and α_c is the covalency of the material of interest given by $\alpha_c = \left(1 - \alpha_p^2\right)^{1/2}$. Figure 5 plots the calculated ε_∞ and ε_o for various N-content in $Al_{0.05}Ga_{0.95}As_{1-y}N_y$, where both ε_0 and ε_∞ (then n) increase with the N-proportion increasing in the range 0.01 to 0.04, whereas the fundamental gap decreases dramatically in this range.

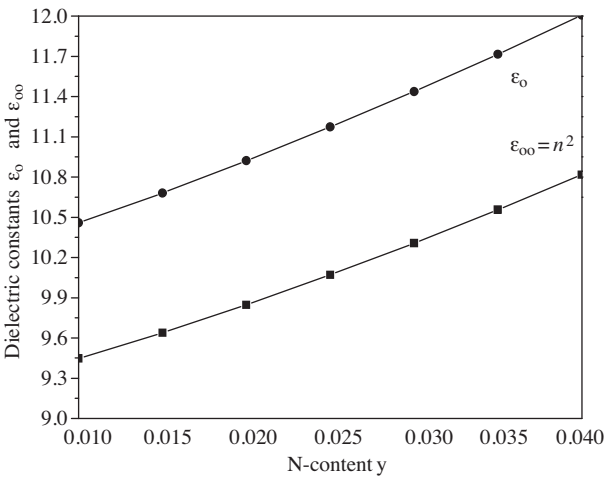

Figure 5. Static and high frequency dielectric functions (respectively ε_o and ε_∞) both as a function of various N-content (up to 4%) for $Al_{0.05}Ga_{0.95}As_{1-y}N_y$ alloys.

3. Approximate quantized energy levels in $Al_xGa_{1-x}As_{1-y}N_y/GaAs$ QW lasers

QW lasers have been developed extensively since they exhibit many advantages, such as very low threshold current densities, high coupling efficiencies into optical fibre, single mode operation narrow static and dynamic linewidth, high output power, large modulation bandwidth, and high lasing temperature [23]. The design optimization of the QW lasers requires a large degree of numerical computation because there are several laser parameters involved such as the quantum well/barrier composition, the number of QWs, the cavity length and the facet reflectivity [23]. The basic properties of AlGaNAs /GaAs materials are of great technological interest and the choice of varying N fraction has provided the flexibility of controlling both electronic and optical properties [6]. So as to calculate the optical transition wavelength between the quantized energy levels in the AlGaAsN/GaAs heterostructure, a schematic energy band diagram for a typical QW structure is shown in Figure 6, where respectively, ΔE_c and ΔE_v are the discontinuities of the band edges of conduction and valance bands at the heterojunction, E_{cn} and E_{vn} the energy levels in CBs and VBs, E_g and E_{tr} (which equals to $E_g + E_{vn} + E_{cn}$) are the band gap energy and the transition energy between the two quantized energy levels, E_{fc} and E_{fv} are the quasi-Fermi levels for electrons and holes in the well. Assuming that the quantized levels for holes E_{vn} are measured from the top of the VB down into the VB and using the parabolic band model [24], we can obtain E_{vn} by solving the following eigenvalue equations:

$$\frac{m_{vb}}{m_{vw}}\sqrt{\frac{\Delta E_v - E_{vn}}{E_{vn}}} = \left\{ \begin{array}{l} \tan \\ -\cot \end{array} \right\} \left(\frac{W\sqrt{2m_{vw}E_{vn}}}{2\,\hbar}\right) \left\{ \begin{array}{l} n : even \\ n : odd \end{array} \right\} \tag{14}$$

with $\hbar = h/2\pi$ the Planck's constant, W the well width, m_{vw} and m_{vb} the effectives masses of holes inside of the well and the barrier, respectively. If $\Delta W_v = \left(\frac{2\,\hbar}{\sqrt{m_{vw}}}\right) / \sqrt{\Delta E_v \frac{m_{vw}}{m_{vb}}}$ and $\Delta E_v >> E_{vn}$, this later is expressed by [23, 24]

$$E_{vn} = \frac{\left[\frac{(n+1)\pi}{2} \frac{2\,\hbar\ /\sqrt{2m_{vw}}}{w+\Delta W_v}\right]^2}{1 + \left[\frac{(n+1)\pi}{2}\right]^2 \frac{m_{vw}}{m_{vb}} \left[\frac{\Delta W_v}{w+\Delta W_v}\right]^3} \tag{15}$$

It should be noted that (15) is an accurate solution to (14) when ΔE_v becomes infinity:

$$E_{vn} = \left[\frac{(n+1)\,\pi}{2} \frac{2\,\hbar\ /\sqrt{2m_{vw}}}{w}\right]^2 \tag{16}$$

If we neglect the $(\Delta W_v)^3$ term in (15), we can interpret $(W + \Delta W_v)$ as an effective well width, where ΔW_v is induced by a finite barrier height ΔE_v. The energy levels E_{cn} for the CB are expressed by (15) if we replace the subscript v by c[23, 24]. We have calculated the subband energies for the VB as a function of $Al_xGa_{1-x}N_yAs_{1-y}$ well widths, which are plotted in Figure 7. For the limit when the well width reduces to zero, the first subband energy for the BV approaches the limit of the VB-edge discontinuity ΔE_v, whereas, the number of energy levels increases with the well width increasing. However, if the barrier width W_b is extremely large the Tunnel effect decreases and the QWs constituting the laser structure act independently. Note that the duplication of the levels (Figure 7) is due to the Tunnel effect which decreases for an extremely large barrier

width. In other hand, the variation of the effective masses shows the effects of the *strain* on the QW laser performances, which has important applications to optoelectronic and electronic devices [24, 25].

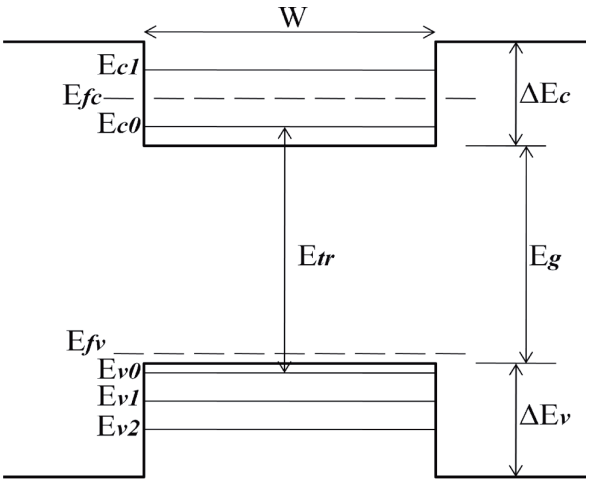

Figure 6 Band model for a quantum well structure.

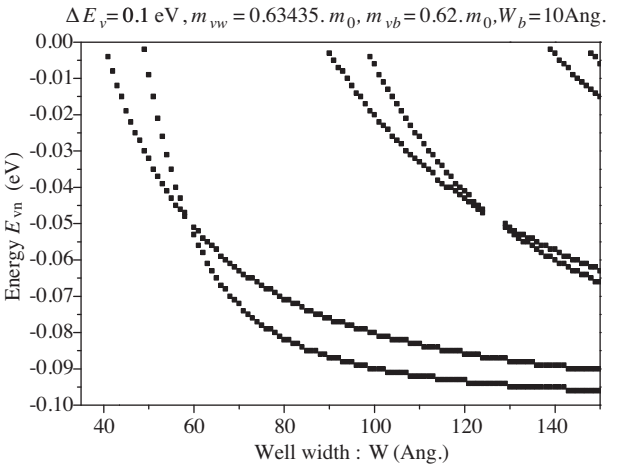

Figure 7. Quantized energy levels in the valence band (E_{vn}) of $Al_xGa_{1-x}As_{1-y}N_y$ quantum wells as a function of the well width (W).

The desired transition wavelength corresponding to the transition between quantized levels, based on equation 16, can be expressed as

$$\lambda_n(\mu m) = \frac{1.24}{(E_0 + E_{cn} + E_{vn}) : (eV)} \tag{17}$$

In Figure 8, we have plotted the calculated λ_0 and λ_1, respectively for the first (1^{st}) and second (2^{nd}) transitions ($n = 0;\ 1$) between electrons and heavy holes levels as a function of the well width for the $Al_{0.05}Ga_{0.95}N_{0.04}As_{0.96}$ (well)/GaAs (barrier) QW structure. The two curves to correspond the numerically calculated values of the wavelength by neglecting $(\Delta W_i)^3$ $(i = c, v)$ in (15) for both 1^{st} and 2^{nd} transition and corresponding to the used parameter values [26, 27] in the calculation, as listed in Table 3. The simulation results suggest that the AlGaAsN system has proved its high potential for applications in GaAs-based telecom lasers in the 1.3 μm range for an active layer width up to 20 nm. Knowing the GaAs, AlAs, GaN and AlN VB offsets of respectively –0.8, –1.33, –2.64 and –3.44 eV [28], a VB offset value for $Al_{0.05}Ga_{0.95}N_{0.04}As_{0.96}$ of –0.9 eV is adopted and a VB-edge discontinuity with GaAs of $\Delta E_v = 0.21\ \Delta E_g$ is assumed.

Table 3. Parameter values used in the wavelength calculation.

Parameters	$Al_{0.05}Ga_{0.95}N_{0.04}As_{0.96}$	GaAs
Band gap (eV)	0.941^a	1.424^d
Electron effective mass (in m_0 units)	0.0761^b	0.0665^e
Heavy hole effective mass (in m_0 units)	0.6343^c	0.62^f

Note: ^{a,b,c}This work with data of ref. [3], ref. [26] and ref. [27]; ^{d,e}ref. [26] ; ^{f}ref. [27].

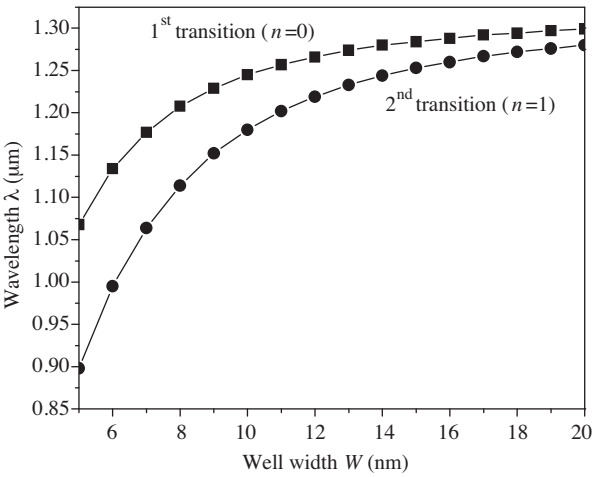

Figure 8. Wavelengths corresponding to the first (1^{st}) and second (2^{nd}) transitions between the quantized energy levels of conduction electrons and heavy holes as a function of the well width calculated for $Al_{0.05}Ga_{0.95}As_{0.96}N_{0.04}$ (well) and GaAs (barrier).

4. Conclusion

Using the EPM method under the VCA approximation, we have successfully studied the effect of N content on electronic and optical properties in zinc-blende $Al_xGa_{1-x}N_yAs_{1-y}$ alloys with N-fraction ranging from 1 to 4%, used as thin films in QW lasers. A study of the band structures versus N mole composition revealed that all these narrower band gap alloys with Al mole fraction of 5% should have an indirect band gap. It has been shown that the band gap energies of these alloys calculated by the EPM method can be obtained by a good agreement with those of the BAC model, especially for $y \leq 2\%$. $\Delta E_v = 0.21\Delta E_g$ of $Al_{0.05}Ga_{0.95}N_{0.04}As_{0.96}$ /GaAs is assumed and analytical expressions derived for the quantized energy levels have been show to provide not only an efficient way of computing the optical transition wavelength between these quantized levels of electrons and holes in QWs but also a convenient way of designing the $Al_xGa_{1-x}N_yAs_{1-y}$ QW lasers for which the analytical approach is expected to show its significant advantage for tuning the emission wavelength in the near infra-red range until 1.3 μm.

References

[1] Shuji Nakamura, *J. Vac. Sci. Technol.*, **A 13**, (1995), 705.

[2] J. Wu, W. Walukiewicz, K. M. Yu, J. W. Ager III, S. X. Li, E. E. Haller, Hai Lu, William J. Schaff, *Solid State Commun.*, **127**, (2003), 411.

[3] K. M. Yu, W. Walukiewicz, J. Wu, J. W. Beeman, J. W. Ager III, E. E. Haller, *Appl. Phys. Lett.*, **90**, (2001), 2227.

[4] C. Skierbiszewski, P. Perlin, P. Wisniewski, W. Knap, T. Suski, W. Walukiewicz, W. Shan, K. M. Yu, J. W. Ager, E. E. Haller, J. F. Geisz, J. M. Olson, *J. Appl. Phys.*, **76**, (2000), 2409.

[5] H. P. Xin, K. L. Kavanagh, M. Kondow, C. W. Tu, *J. Cryst. Growth*, **201/202**, (1999), 419.

[6] D. N. Talwar, *J. Appl. Phys.*, **99**, (2006), 123505-1.

[7] K. Yamamoto, M. Uchida, A. Yamamoto, A. Masuda, A. Hashimoto, *Phys. Stat. Sol (b)*, **234**, (2002), 915.

[8] A. Hashimoto, T. Kitano, K. Takahashi, H. Kawanishi, A. Patane, C. T. Foxon, A. Yamamoto, *Phys. Stat. Sol (b)*, **228**, (2001), 283.

[9] J. Wagner, T. Geppert, K. Kohler, P. Ganser, M. Maier, *Appl. Phys. Lett.*, **83**, (2003), 2799.

[10] W. Shan, W. Walukiewicz, and J. W. Ager III, E. E. Haller, J. F. Geisz, D. J. Friedman, J. M. Olson, and S. R. Kurtz, *Phys. Rev. Lett.*, **82**, (1999), 1221.

[11] J. D. Perkins, A. Mascarenhas, Yong Zhang, J. F. Geisz, D. J. Friedman, J. M. Olson, and Sarah R. Kurtz, *Phys. Rev. Lett.*, **82**, (1999), 3312.

[12] W. Shan, K. M. Yu, W. Walukiewicz, J. W. Ager III, E. E. Haller, M. C. Ridgway, *Appl. Phy. Lett.*, **75**, (1999), 1410.

[13] W. Shan, W. Walukiewicz, J. W. Ager III, E. E. Haller, J. F. Geisz, D. J. Friedman, J. M. Olson, Sarah R. Kurtz, *J. Appl. Phys.*, **86**, (1999), 2349.

[14] I. Vurgaftman, J. R. Meyer, *J. Appl. Phys. Lett.*, **94**, (2003), 3675.

[15] T. Matilla, S. Huai-Wei and A. Zunger, *Phys. Rev. Lett.*, **B60**, (1999), R11245.

[16] H. Aourag, B. Bouhafs, M. Certier, *Phys. Stat. Sol (b)*, **201**, (1997), 117.

[17] K. Kassali, N. Bouarissa, *Microelectron. Eng.*, **54**, (2000), 277.

[18] H. Abid, N. Badi, M. Driz, N. Bouarissa, K. H. Benkabou, B. Khelifa, H. Aourag, *Microelectron. Eng.*, **B 33**, (1995), 133.

[19] Seong Jae Lee, Tae Song Kwon, Kyun Nahm and Chul Koo Kim, *J. Phys. Condens. Matter*, **2**, (1990), 3253.

[20] M. Gungerich, P. J. Klar, W. Heimbrodt, K. Volz, K. Kohler, J. Wagner, A. Polimeni, M. Capizzi, H. Ch. Alt, Y. V. Gomeniuk, *Phys. Stat. Sol (c)*, **3**, (2006), 619.

[21] S. Yu. Davydov and S. K. Tikhonov, *Semiconductors*, **32**, (1998), 947.

[22] P. Vogl, *J. Phys. C: Solid State Phys.*, **11**, (1978), 251.

[23] Toshihiko Makino, *IEEE J. Quantum Electron.*, **32**, (1996), 493.

[24] M. Asada, A. Kameyama, Y. Suematsu, *IEEE J. Quantum Electron.*, **QE-20**, (1984), 745.

[25] Shun Lien Chuang, *Phys. Rev. Lett.*, **B 43**, (1991), 9649.

[26] Peter J. Klar, *Prog. Solid State Chem.*, **31**, (2003), 301.

[27] H. Mathieu, Physique des Semiconducteurs et des composants électroniques, ed. 5, (Dunod, Paris, 2005), p. 31.

[28] I. Vurgaftman, J. R. Meyer and L. R. Ram-Mohan, *J. Appl. Phys.*, **89**, (2001), 5815.

[29] D. E. Aspnes, C. G. Olson and D. W. Lynch, *Phys. Rev. Lett.*, **37**, (1976), 766.

[30] T. Lei, M. Fanciulli, R. J. Molnar, T. D. Moustakas, R. J. Graham and J. Scanlon, *Appl. Phys. Lett.*, **59**, (1991), 944.

[31] B. Monemar, *Phys. Rev. Lett.*, **B 8**, (1973), 5711.

[32] W. M. Yim, E. J. Stofko, P. J. Zanzucchi, J. I. Pankove, M. Ettenberg, S. L. Gilbert, *J. Appl. Phys.*, **44**, (1973), 292.